Smoke buildup and light scattering in a cylindrical cavity above a uniform flow.

Abstract

In this study, we use computational fluid dynamics (CFD) and aerosol dynamics modeling to investigate the buildup of smoke and light scattering in a cylindrical cavity geometry, considered to be an idealized representation of a photoelectric smoke detector. CFD coupled with the quadrature method of moments (QMOM) is used for simulation of aerosol dynamics. The Rayleigh-Debye-Gans/Polydisperse Fractal Aggregate (RDGPFA) theory is used for calculation of smoke extinction and angular light scattering. It is seen that the flow external to the cavity sets up a recirculating flow pattern within the cavity and that the flow processes determine the spatial distribution of smoke. Aerosol extinction and scattering calculations are performed to examine the time varying profiles of the intensity along a simulated LED light beam and the scattered intensity at different angles. The variation of the detector activation time with inlet velocity and smoke volume fraction is obtained from a calculation of the angular light scattering. The results are compared with calculations using an empirically determined detector response function and with a simpler model that assumes a uniform distribution of smoke inside the cavity. Results indicate that although the distribution of smoke inside the cavity is not uniformly mixed, the simple first order mixing model with appropriately chosen parameters is valid for predicting detector activation time.

Keywords: smoke detector, CFD simulation, smoke entry, light scattering, detector activation time.

Nomenclature

a Primary particle radius (m).

A Equivalent inlet area for plug flow (m^2).

A_s Cross sectional area of scattering volume (m^2)

C_s Mass concentration of smoke (kg/m^3).

$D(r)$ Diffusivity of particles of radius r (m^2/s).

D_f Fractal dimension.

$E(m)$ Factor for absorption $E(m) = \mathrm{Im}\left(\dfrac{m^2 - 1}{m^2 + 2} \right)$

$F(m)$ Factor for scattering $F(m) = \left| \dfrac{m^2 - 1}{m^2 + 2} \right|^2$

f_v Volume fraction.

$\bar{f}_v$ Volume fraction averaged over the cavity.

g Acceleration due to gravity (m/s^2).

I Light intensity (W/m^2).

k Wave number ($\dfrac{2\pi}{\lambda}$) (m^{-1}).

k_B Boltzmann constant (JK^{-1})

k_f Fractal prefactor.

K_{ext} Extinction coefficient (m^{-1}).

L_e Characteristic length (m).

m Complex index of refraction of soot $(m = 1.54 + 0.48i)$.

$\dot{m}$ Mass flow rate (kg/s).

M_m m$^{\text{th}}$ moment of the size distribution.

$n(v)$ Size density function (# of particles of volume v/m^3 of gas).

N Number of primary particles per aggregate.

N_Q Number of quadrature points.

p Output voltage of the detector (microvolts).

P Power scattered to the detector (Watts).

P' Power at the detector per unit power of the LED source.

q Scattering wave vector $q = \dfrac{4\pi}{\lambda}\sin\left(\dfrac{\theta}{2}\right)$ (m^{-1}).

r Distance to the detector from the scattering element (m).

r_v Volume equivalent radius of the fractal aggregate (m).

R Radius of the cylindrical cavity (m).

$R_{\text{det}}(d)$ Detector response function (microvolts cm^3).

R_g Radius of gyration (m).

s Coordinate along the path of incident light beam (m).

T Temperature of the fluid $T = 300K$.

t_e Smoke entry time lag (s).

U Inlet velocity (m/s).

U_t Terminal settling velocity (m/s).

v Total volume of the soot agglomerate (m^3).

$\vec{v}$ Flow velocity vector (m/s).

V Volume (m^3).

W Quadrature weight (#/m^3).

Subscripts / superscripts

~,'   Dummy variable (for integration).

abs   Absorption.

act   Detector activation.

cav   Cavity.

coag   Pertaining to coagulation.

cr   Threshold value (for detector activation).

det   Detector.

diff   Pertaining to diffusion.

e, ∞ External to the smoke detector.

flow   Pertaining to the flow.

i, j Pertaining to the ith or jth quadrature point / weight.

mix   Mixing model.

p Pertaining to the primary particle of the soot agglomerate.

settling   Pertaining to gravitational settling.

scat   Scattering.

$s, s\infty, sr$ Pertaining to smoke inside the detector, outside the detector and at detector

        activation respectively.

v Used to define the volume equivalent radius r_v.

Greek symbols

β Coagulation kernel (m^3).

λ Wavelength of incident beam $(\lambda = 632nm)$.

μ Viscosity of the fluid (Pa s).

θ Angle with respect to the incident beam in the scattering plane.

ρ Density of soot (kg/m^3).

σ Cross section (m^2).

τ Time scale (seconds).

Ω Solid angle (steradians).

1. Introduction

Smoke detectors have been credited as being the single most influential technology in reducing the number of fire deaths over the past 30 years. The accurate detection of a fire often means the difference between safe egress and potentially life threatening conditions for people caught in structure fires. Consequently, during the simulation of a fire scenario, the accurate prediction of the response of smoke detectors is crucial. Due to the scale and complexity of a fire event, methods for detector activation prediction have mostly relied on empirical techniques. A widely used method is the temperature correlation and the response time index (RTI) method (Heskestad and Delichatsios (1977), Benjamin et. al. (1979)). The temperature correlation method is based on the

reasoning that heat generation and transport from a burning material to a sensing location is analogous to the smoke generation and transport from the fire to the sensor and therefore the temperature and smoke concentration must be correlated. The response is predicted using the RTI which is a measure of the sensitivity of the detector to temperature changes. Generally a temperature rise of 13°C above the ambient is used as the criteria for detector activation. The shortcomings of this approach have been discussed by Bukowski and Averill (1998). For effective detection of a fire one needs to accurately determine the total time associated with the ignition and growth of the fire, transit of the smoke or other combustion byproducts to a detector and the detector activation time. Simplified physical arguments have been used to derive correlations for the time scales associated with all of the above phenomena. A summary of these correlations is presented by Newman (1987). In particular, an empirical correlation for the detector response time based on a detector response function is given in Mulholland and Liu (1981). The correlation is developed for a particular smoke detector model. One of the objectives of this study is to compare detector response times obtained using this correlation with direct simulations. More detailed treatment like Computational Fluid Dynamics (CFD) can provide a more accurate prediction of fire detection times (Ierardi and Barnett (2003)). However detailed models involving the coupled flow field and aerosol dynamics effects are only recently being considered (e.g. Snegirev et al. (2001)).

For an understanding of activation for a particular type of detector it is appropriate to focus on the smoke/aerosol properties (concentration, size distribution, index of refraction etc.) in the vicinity of the detector. The most widely used model for smoke detector activation assumes that activation is dependent only on the smoke concentration

within the sensing chamber/volume inside the smoke detector housing. The sensing chamber/volume smoke concentration is modeled as a first order system that is coupled to an external smoke concentration with a time lag (e.g. Cleary et al. (2000)). A schematic of this model is shown in Fig. 1.

$$\frac{dC_s}{dt} = \frac{1}{\tau_{mix}}\left(C_{so}(t-t_e) - C_s(t)\right); t \geq t_e \tag{1}$$

In equation (1) $C_s(t)$ is the smoke mass concentration inside the sensing chamber at time t and $C_{s\infty}$ is the smoke concentration external to the detector housing at an earlier time $t-t_e$. There are two time parameters t_e and τ_{mix} in (1). The parameter t_e denotes the time lag that is associated with the entry and penetration of the smoke into the sensing chamber of the detector. Depending on the detector design, smoke has to be transported through an external detector housing consisting of filters, baffles and other obstacles used to block stray light (in the case of photoelectric detectors) from entering the sensing chamber. A model suggested by Heskestad (1975) is to use a plug flow model over an equivalent length scale, L_e. The entry time is given by

$$t_e = \frac{L_e}{U_e} \tag{2}$$

The second time constant τ_{mix} gives the mixing time or the time scale required for smoke concentration to reach the threshold for detector activation. Both these parameters depend on the geometry as well as the size distribution of the smoke and local convection velocity through the detector. If we assume that the external smoke concentration is constant then (1) can be integrated to give

$$\frac{C_s(t)}{C_{s\infty}} = 1 - \exp\left(\frac{-(t-t_e)}{\tau_{mix}}\right) \quad t \geq t_e \tag{3}$$

$$\frac{C_s(t)}{C_{s\infty}} = 0 \quad t < t_e$$

It may be possible to scale the mixing time parameter, τ_{mix}, with the inlet velocity as

$$\tau_{mix} = \frac{L_{mix}}{U_e} \tag{4}$$

where L_{mix} is a characteristic mixing length scale. One of objectives of this work is to test

this hypothesis and determine L_{mix} using (4).

Another quantity of interest in detection is the extinction coefficient and it is usually

assumed that the extinction coefficient is proportional to the concentration. Experimental

characterization of smoke detectors involves the determination of the two time

parameters (t_e and τ_{mix}) or the length scale L_{mix} and threshold concentration $C_{sr}(t_r)$ by

assuming a fit of the form (2) or (3) from which t_e and τ_{mix} can be calculated (e.g.

Bjorkman et al. (2002); Cleary et al. (2000)). In spite of the numerous experimental

studies to characterize smoke detectors, the theoretical study of these processes remains a

difficult task. This is due to the fact that smoke detector geometries as well as the physics

associated with the detection process are complicated. Nevertheless, due to differences in

design and the practical difficulties in experimentally characterizing each brand, a

theoretical analysis of detector response involving first principles is clearly necessary.

Due to advances in CFD and aerosol dynamics modeling, it is gradually becoming

feasible to study smoke entry and build up as well as predicting detector response

theoretically. Once a standardized methodology is available manufacturers can evaluate different designs without the need for expensive testing.

In this work we focus on some basic phenomena that are important in most detectors of the photoelectric type. We perform a CFD study coupled with aerosol dynamics of the smoke accumulation in the sensing chamber. Due to the extreme variations in design, we ignore the time constant associated with smoke entry, t_e, and instead focus on the mixing process (i.e. the time scale τ_{mix}). We also present a calculation for the extinction coefficient and the angular distribution of light scattering from fractal agglomerates. Although we have chosen a simplified geometry, the purpose is to illustrate analytical methods that can be adapted to a wide range of detector designs.

2.1 Flow and aerosol model

In this section we briefly describe the CFD model and the aerosol equations. A simplified geometry is used to model the smoke detector system (cf. Fig. 2). The computational grid shown in Figure 2 is generated using the software Gambit 2.1. Hexahedral meshes are used for both the cavity and the external domain. The flow solver is capable of creating the grid interface between the two domains.

Unlike typical smoke detectors that consist of an external housing enclosing a smaller sensing chamber, we effectively consider a detector whose internal cavity is comprised entirely of the sensing chamber. For simplicity only one half of the detector is considered as the inflow and detector geometry are both symmetric with respect to the vertical plane. The main flow is set up along the x-axis (from –x to +x). The internal cavity has a radius

of 7.5 cm and a height of 10cm. An LED light source and a photodiode are assumed to be placed at an elevation of 5cm (mid-height) within the cavity. The details of the scattering arrangement are given in the next section. Below the cavity, an external flow is simulated in a computational volume that is 20 cm in length, 7.5 cm in width and 4 cm in depth. As mentioned earlier we only consider the flow field at the location of the sensing chamber. The primary flow field induces a secondary recirculating flow within the cavity where the smoke detection takes place. This secondary flow is responsible for transport of the smoke to the location of the LED beam. The light scattered by the particles that are present in the path of the LED beam (i.e. the scattering volume) is detected by a photodiode that is assumed to be placed in the circumference of the cavity. The internal flow within the smoke detector is simulated using a commercial CFD package (Fluent 6.1). The CFD solver has been benchmarked to solve the mass and momentum equations. The aerosol dynamics associated with the problem is considered next.

A user defined function has been included to solve the aerosol general dynamic equation (GDE). The GDE for modeling aerosol dynamics in radius space is,

$$\partial n(r_v)/\partial t + \nabla \cdot n(r_v)\vec{v} = \nabla \cdot D(r_v)\nabla n(r_v)$$

$$+1/2\int_0^{r_v} \beta\left(\tilde{r}_v, (r_v^3 - \tilde{r}_v^3)^{\frac{1}{3}}\right)n(\tilde{r}_v)n((r_v^3 - \tilde{r}_v^3)^{\frac{1}{3}})d\tilde{r}_v - \int_0^{\infty} \beta(r_v,\tilde{r}_v)n(r_v)n(\tilde{r}_v)d\tilde{r} - \nabla \cdot \vec{U}_t(r_v)n(r_v)$$

$$(5)$$

where the state of the particle (fractal aggregate) is assumed to be defined by its volume equivalent radius r_v. In writing the GDE, the term containing the particle current in radius space that includes both the nucleation and surface growth terms is dropped. In the problem that is considered here, we neglect the aerosol physics involving nucleation and condensation. The second term on the left hand side gives the convective transport of the

smoke by the fluid flow. The flow field is obtained from the CFD solver. The first term on the right hand side gives the diffusion of the aerosol, the next two terms model the coagulation and the last term models the gravitational settling. For the problem under consideration, the effects of gravitational settling, diffusion and coagulation were found to be negligible. These aerosol evolution processes are important in the smoke generation and transport phases and ultimately determine the aerosol size distribution at the point of detector entry. The GDE is solved using a Quadrature Method of Moments (QMOM) formulation. A description of the methodology can be found in McGraw (1997). In recent years this method has been extended to a large number of important aerosol phenomena. We refer the reader to McGraw and Wright (2003), Wright, McGraw, and Rosner (2001), Wright (2000), Upadhyay and Ezekoye (2003) and references therein. Modifications of the QMOM called DQMOM (direct quadrature method of moments) and its possible applications in turbulent reacting flow simulation have been discussed in Fox (2003).

The moment equations can be approximately closed once the integrals involving $n(r,t)$ are evaluated by quadrature sums. For the sake of generality the full moment equations are presented below.

$$\partial M_m / \partial t + \nabla \cdot M_m \vec{v} =$$
$$\sum_{i=1}^{N_Q} (\nabla \cdot \nabla D(\bar{r}_{v,i})W_i - \nabla \cdot (\vec{U}_t(\bar{r}_{v,i})W_i))$$
$$+ 1/2 \sum_{i=1}^{N_Q} \sum_{j=1}^{N_Q} [(\bar{r}_{v,i}^3 + \bar{r}_{v,j}^3)^{\frac{m}{3}} - \bar{r}_{v,i}^m - \bar{r}_{v,j}^m] \beta(\bar{r}_{v,i}, \bar{r}_{v,j}) W_i W_j \qquad (6)$$
$$m = 0,1,2,3...$$

where $\bar{r}_{v,i}$ are the quadrature points and W_i are the quadrature weights.

In this work, size dependence of diffusivity and settling velocity is not considered. An equivalent diffusivity and settling velocity evaluated for the average size of the particles

is used. The effective diffusivity and settling velocity, neglecting the slip correction, is

given by $D = \dfrac{k_B T}{6\pi\mu\bar{r}_v}$ and $U_t = \dfrac{4\rho g \bar{r}_v^2}{18\mu}$ respectively. For the size of the particles

considered, the settling velocities are found to be much smaller than the smallest flow

velocities encountered in the problem and thus gravitational settling is neglected. For

instance for the typical particle sizes considered in this work, the diffusivity is in the

order of 10^{-11}m^2/s settling velocity is in the order of 10^{-5} to 10^{-6} m/s. Taking the radius of

the cavity as a characteristic length scale, the characteristic time scales for diffusion,

$\tau_{diff} \sim \dfrac{R^2}{D}$ is of the order of 10^8 seconds. The characteristic time for settling,

$\tau_{settling} \sim \dfrac{R}{U_t} \sim 10^4$ seconds. Both these time scales are much smaller than the minimum

flow convective time scale, $\tau_{flow} \sim \dfrac{R}{U} \sim 10^2$, considered in this study. The continuum

Brownian kernel for fractal aggregates is used. β for collision of two particles of volume

v_i and v_j is given by $\beta = \dfrac{2k_B T}{3\mu}\left(v_i^{1/D_f} + v_j^{1/D_f}\right)\left(v_i^{-1/D_f} + v_j^{-1/D_f}\right)$. Taking an average value

of β, the characteristic coagulation time is given by $\tau_{coag} \sim \dfrac{6\mu}{8k_B T \bar{v} M_0}$. Here M_0 is the

first moment and $\bar{v}$ is the average volume of the aggregates. Calculations show that τ_{coag}

is much greater than any other time scale. As mentioned earlier surface growth and

nucleation effects are not considered. For the smoke detector problem considered in this

work only convective effects are dominant and the aerosol computations are very much

simplified.

The quadrature method of moments first introduced by McGraw (1997) is an increasingly popular method for solving aerosol dynamics problems. This is because unlike other moment methods, there are no assumptions or restrictions on the form of the size distribution function. A further use of the QMOM is that other quantities of interest like the extinction coefficient and the intensity of scattered light can be approximated directly from the moments, M_m, that are obtained using (6). Although for this particular problem, we see that the coagulation, diffusion and sedimentation terms are negligible, and the full capabilities of QMOM are not utilized, QMOM nevertheless appears to be a very useful tool for more sophisticated studies of smoke detectors. The number of quadrature points N_Q to be used in (6) is determined by the required accuracy of the quadrature sum in approximating the integral. The number of quadrature points must also be chosen such that other smoke properties that are approximated by quadrature sums are accurate. In this problem, the size distribution always remains lognormal due to negligible effects of diffusion and coagulation. A lognormal distribution can be completely specified using three moments. The smoke extinction coefficient and the angular intensity involve integration over the lognormal distribution and both are found to be accurately evaluated using two quadrature points. Therefore, in this study the two-point quadrature scheme ($N_Q = 2$) is used and the four moments M_0, M_1, M_2, M_3 are tracked.

2.2 Light scattering

The photoelectric detector works on the light scattering principle. A light source typically a light emitting diode emits a beam towards a light stop. An alarm activation detector,

typically at some angle to the beam in the scattering plane, measures light scattering to determine the presence of smoke particles. The geometry to be considered for the scattering model is shown in Fig. 3. The scattering arrangement is similar to that used in experimental studies of a photoelectric detector (e.g. Weinert et al. (2003)). A light beam from an LED source is shone across the chamber. If particles are present in the chamber, they scatter light. The light scattered by the particles is incident on detectors placed on the periphery of the cavity. For this analysis we take an LED beam incident in a horizontal plane at the mid-height of the cylindrical cavity and calculate the angular scattering distribution along the outer circumference.

Light scattering from irregular particles is a complicated phenomenon. A complete characterization of the light scattered from soot or smoke requires the solution of Maxwell's equations. Due to the complexity of these equations, they have only been carried out for some basic shapes. However a simplification exists for computation of light scattering due to soot produced from flaming fires. In this case, it has been shown that the structure of soot aggregates is fractal (e.g. Sorensen et al. (1992)). It has also been shown that for these aggregates, the Rayleigh-Debye-Gans approximation is applicable (see for example Farias et al. (1995), Sorensen (2001)). The Rayleigh-Debye-Gans-Polydisperse-Fractal-Aggregates (RDGPFA) approach considerably simplifies computations of the absorption and extinction properties of soot agglomerates as shown below. It must be mentioned that this approximation is valid only for soot produced from typical flaming fires. For smoke generated from smoldering combustion or other nuisance aerosols, this approximation is not valid as can be seen from the degree of polarization measurements presented in Loepfe et al. (1997) and Weinert et al. (2003). Computations

using the more complicated Mie theory are only recently being carried out (Sorensen (2000). In the following we briefly develop the equations for the absorption and scattering coefficients for fractal aggregates and present a methodology for computation of angular light scattering.

2.2.1 Extinction

First the incident intensity along the LED light beam needs to be established. The general theory uses the total absorption and scattering cross sections. A soot cluster consists of a number of spherical primary particles distributed in a fractal cluster. The primary particles are assumed to be Rayleigh absorbers and scatterers. The total absorption cross section for an aggregate is the sum of the absorption cross sections of the Rayleigh particles (Nelson (1989)).

$$\sigma_{abs} = 4\pi N k a^3 E(m) \tag{7}$$

In this equation N is the number of primary particles per aggregate, a is the primary particle radius and m is the complex index of refraction for soot. In this work, m is taken to be $1.54 + 0.48i$. This value is reported in Koylu and Faeth (1996) for soot generated by turbulent diffusion flames of hydrocarbon fuels. It is also mentioned that the refractive index is relatively independent of the type of fuel in the visible and infrared spectrum. The differential scattering cross section is not simply the sum of the scattering cross sections of the individual Rayleigh particles because one has to consider the interference of light scattered by the individual primary particles. These effects are modeled by the use of a structure factor which contains the information about the spatial arrangement of

the primary particles within the cluster. It is a function of the scattering wave vector, q

and a characteristic size of the cluster usually taken to be the radius of gyration, R_g. The

differential scattering cross section for incident unpolarized light is then written as

(Sorensen (1997))

$$\frac{d\sigma_{scat}}{\partial\Omega} = N^2 k^4 a^6 F(m)\left(\frac{1+\cos^2\theta}{2}\right)S(qR_g) \tag{8}$$

$$S(qR_g) = \left(1+\left(\frac{2}{3D_f}\right)q^2 R_g^2\right)^{\frac{-D_f}{2}} \tag{9}$$

where $S(qR_g)$ is the structure factor. Various forms of the structure factor have been

proposed in the literature. However they are not too different and for the sake of

simplicity, the Fischer-Burford form (9) is used in this study. The differential scattering

cross section multiplied by the incident intensity gives the fraction of the total power

scattered in a particular solid angle and hence is an important quantity in the study of

angular light scattering. The total scattering cross section can be found by integrating

over all solid angles. Details of the integration can be found in Sorensen (1997).

$$\sigma_{scat} = \int_0^{2\pi}\frac{d\sigma_{scat}}{d\Omega}d\theta\int_0^\pi\sin^3\phi d\phi = \frac{8\pi}{3}N^2 k^4 a^6 F(m)G(kR_g) \tag{10}$$

where

$$G(kR_g) = (1+\left(\frac{4}{3D_f}\right)k^2 R_g^2)^{\frac{-D_f}{2}} \tag{11}$$

The differential scattering cross section depends on θ. The integration in equation (9) is

non-trivial because the expression for the structure factor, which has a θ dependence, is

usually complicated. To carry out this integration, the relatively simpler Guinier form

($S(q) = 1 - \dfrac{q^2 R_g{}^2}{3}$) of the structure factor that is valid for small qR_g was used. The result

was then modified to get an expression, $G(kR_g)$, that is valid for the entire range of qR_g.

This approach is similar to the one used by Dobbins and Megaridis (1991) with the slight

difference that our computation involves unpolarized incident light. Expressions (7) and

(8) have been obtained for a cluster of a particular size. For a polydisperse population of

aggregates, the expressions need to be integrated over the entire size distribution. The

size dependencies are contained in N and R_g. In our calculations we have chosen the

volume equivalent radius as the size parameter. The volume of the fractal cluster can thus

be obtained and from it the two quantities.

$$N = \frac{v}{v_p} = \left(\frac{r_v}{a}\right)^3 ; v_p = (4/3)\pi a^3 \tag{12}$$

$$R_g = a\left(\frac{N}{k_f}\right)^{\frac{1}{D_f}} \tag{13}$$

The values of the fractal prefactor ($k_f = 2.44$) and fractal dimension ($D_f = 1.8$) are

taken from Koylu and Faeth (1994). The extinction for the entire population is

determined by integrating over the size distribution. A particularly nice feature of the

quadrature method of moments is that integrals over the size distribution can be easily

and accurately approximated by quadrature sums. The value for the local population

averaged extinction coefficient is then evaluated as

$$\overline{K}_{ext} = \int_0^\infty (\sigma_{scat}(r_v) + \sigma_{abs}(r_v))n(r_v)dr_v = \sum_{i=1}^{N_Q} (\sigma_{scat}(r_{v,i}) + \sigma_{abs}(r_{v,i}))W_i \tag{14}$$

Once the total absorption and scattering cross sections and the extinction coefficient have been determined, the intensity along the path length of the light beam can be easily found using an application of the Beer Lambert law.

$$I(s) = I_0 \exp\left(-\int_0^s \overline{K}_{ext}(s')ds' \right) \qquad (15)$$

Computational results show that extinction is negligible for detector activation studies and attenuation along the LED beam can be ignored.

2.2.2 Angular light scattering

Finally we can now calculate the angular variation of the scattered light intensity. The geometry for the light scattering is shown in Fig. 3. In our analysis, the scattering plane is a horizontal plane at the mid-height of the cylindrical cavity. A source of coherent, monochromatic light of wavelength, λ, equal to 632nm (usually a Light Emitting Diode (LED)) is placed at one location at the circumference such that the beam is along a diameter. The diameter of the LED beam is assumed to be equal to the width of a computational cell (i.e. 5mm). In practice there could be a divergence of the beam from the LED. In that case the scattering volume becomes a conical region and light scattering computations must be carried out over all the cells lying in the scattering volume. In this study, the LED beam is assumed to be collimated.

An internet survey of different smoke detector designs revealed that there is a wide variation in the beam divergence as well as the wavelength of the LED. In most cases the beam divergence is quite small (around 10°-15°). Further as most of the scattering into

the detector comes from the scattering volume close to the LED beam, the usually small angular divergence is ignored in this study. The beam diameter of 5mm is chosen by measuring the width of the aperture for a particular smoke detector model. The wavelength of 632 nm is characteristic of a red LED and also corresponds to the standard He-Ne lasers used by various researchers.

In the baseline case, a detector is placed at some angle of $20°$ to the incident beam. The total intensity on a detector placed at an angle θ with respect to the center is given by the intensity scattered in that particular angle by all the particles along the LED beam. Consider a region at a distance s' along the beam. The intensity incident on it can be found from (15). For a single particle, the power scattered per solid angle at angle $\theta' = \theta(s')$ is given by $I(s')\dfrac{d\sigma_{scat}}{d\Omega}$ where $\dfrac{d\sigma_{scat}}{d\Omega}$ is evaluated at θ'. The power received by the detector at the fixed angle θ ($\theta(s' = R)$ as shown in Figure 3) is given by

$I(s')\dfrac{d\sigma_{scat}}{d\Omega}\left(\dfrac{A_{det}\cos(\theta - \theta')}{r(s')^2}\right)$. Also accounting for the polydispersity of the scattering particles, we get the scattered power at angle θ by particles at spatial location s' and within the scattering volume $A_s ds'$ as

$$dP(\theta) = I(s')k^4 a^6 F(m)\left(\frac{1 + \cos^2(\theta')}{2}\right)\left(\frac{A_{det}\cos(\theta - \theta')}{r(s')^2}\right)\int_0^\infty N(r_v)^2 S(qR_g(r_v))n(r_v)dr_v A_s ds'$$

(16)

The total power at angle θ is found by summing over the contributions from all the particles along s'.

$$P(\theta) = \int_{s'=0}^{2R}\left[I(s')k^4 a^6 F(m)\left(\frac{1 + \cos^2(\theta')}{2}\right)\left(\frac{A_{det}\cos(\theta - \theta')}{r(s')^2}\right)\int_0^\infty N(r_v)^2 S(qR_g(r_v))n(r_v)dr_v\right]A_s ds'$$

(17)

To evaluate detector response characteristics, the criteria used for detector activation is taken to be the power at the detector per unit power of the LED given by

$$P'(\theta) = \frac{P(\theta)}{I_0 A_s} \qquad (18)$$

In deriving (16) we are assuming that there is no intercluster scattering and the scattered intensity travels to the detector without any attenuation. This is justified because the smoke volume fraction within the detector is usually sufficiently small given that the detector would sound before the concentration levels become high enough for intercluster multiple scattering. As described later, our choice of the critical power for detector activation gives an optical thickness less than 10^{-3}. The medium is certainly optically thin up to the moment at which the detector sounds. The evaluation of the scattered power received at the detector is as far as one can go in the prediction of the activation time from first principles. The alarm threshold is set by the electronics of the photodiode, which varies between different manufacturers.

3. Simulations and results

Simulations of the smoke entry, accumulation and detection are carried out for a range of flow velocities and particle volume fractions. A plug flow velocity profile is used as the input boundary condition at the location $x = -0.1$ m (in Fig. 2). The flow is simulated using a commercial CFD package (Fluent 6.1). Taking the radius of the cavity as a characteristic length scale, the maximum Reynolds number is around 3000. The main flow is essentially an external flow past a flat plate. The velocities inside the cavity are even smaller. Therefore for all the velocities considered the flow is laminar. The

boundary conditions used in the simulation are summarized in Table 1. For the particles, the inlet condition is a fixed lognormal distribution of fractal particles characterized by the volume equivalent radius. The geometric mean volume equivalent radius and the geometric standard deviation are taken to be 0.15 μm and 2 respectively for a wide range of volume fractions. For fractal aggregates, the mean radius of 0.15 μm corresponds to $N = 400$ for a primary particle radius, $a = 20nm$. For this N and with $D_f = 1.8$, $R_g = 0.36\mu m$. These values are characteristic of soot produced from flaming hydrocarbon fuels and have been reported in Koylu and Faeth (1994). To predict the detector response we assume that an LED shines across the cavity diameter at the plane of symmetry (y = 0) and at the mid height (z = 0.05m). A detector is assumed to be placed at the circumference at an angle of 20° to the incident beam. The scattered field is calculated using a series of steps. First a steady state flow profile is obtained from the CFD calculation. Then the aerosol calculations are carried out in a time dependent manner in the presence of the steady velocity profile. The outputs of the calculation are the temporally and spatially varying moments of the particle size distribution. The moments along the spatial direction of the incident LED beam are used in the scattering analysis to determine the scattered intensities at the light detector location.

3.1 Features of the flow field

The flow is predominantly responsible for transport of smoke into the detector and hence we include a brief description of the flow field. The flow field generated inside the cavity at the plane of symmetry due to the outside flow is shown in Fig. 4a. The x- and z-

components of the velocity are shown as a detailed look at the flow field revealed the y-velocity component to be much smaller than the other two. The external flow field is entrained near the base of the cavity and is pushed upwards at the wall. This induces a counterclockwise recirculating flow inside the cavity. The same type of profile was observed at different vertical planes parallel to the one shown. Fig. 4b shows the component of the velocity along the z-direction that is responsible for transporting the smoke into the sensing chamber. Almost all the particles enter at the right and are transported up. Fig. 5 shows the x-y velocity vectors at four different horizontal planes inside the cavity. These velocity components are responsible for horizontally dispersing the particles that are transported inside by the vertical (z-) velocity. Near the base of the plane and slightly upward the flow is in the +x direction. At a certain height the flow reverses due to the recirculation and flows in the – x direction. This motion aids in filling up the cavity uniformly with particles. The same flow features are seen for a wide range of values of the inlet velocity. At very low inlet velocities (~0.001 m/s), the smoke entry process differs. Smoke enters from the left and exits from the right.

3.2 Smoke buildup within the detector

We first examine the buildup of smoke at the scattering volume along the LED beam (y = 0, z = 0.05m). Fig. 6 shows the volume fraction profiles at different times for free stream smoke volume fraction of 10^{-9} and inlet velocity of 0.1 m/s. It is seen that flow processes are largely responsible for the smoke distribution within the cavity. For instance the flow enters the cavity towards the right (close to + 7 cm in Fig. 2) and that is where the smoke

first begins to build up. Some of the smoke is then transported across the detector by the velocity in the –x direction. After the flow loops around the cavity, smoke starts to appear at the opposite end and a second hump begins to grow.

3.3 Light scattering by smoke particles

The angular distribution of the power due to scattering is computed using the methodology outlined in section 2.2. Fig. 7 shows the attenuation of the incident intensity along the LED beam when the inlet volume fraction is 10^{-9} and the inlet velocity is 0.1 m/s. There is very little attenuation in this case. Fig. 8 shows the variation in scattered power with angle along the circumference of the cavity for inlet volume fraction of 10^{-9}. There is a slight increase in the scattered power with time. The strong forward scattering is due to the structure factor and it distinguishes the scattering from fractal aggregates from Rayleigh scattering. There have been numerous experimental measurements of the extinction coefficient of fractal shaped soot aggregates obtained from different hydrocarbon fuels. A check on the computations for the extinction coefficient can be made by comparison with the experimental results compiled in Widmann (2003). The mass specific extinction coefficient can be calculated from (14) as $\sigma_s = \overline{K}_{ext}/\rho, \rho \approx 1.8g/cc$. For the wavelength $\lambda = 632nm$ (and using typical values for the other paramenters), $\sigma_s \lambda = 2.9 \times 10^{-6} m^3 g^{-1}$ while the empirical correlation given by Widmann (2003) is $\sigma_s \lambda = 4.808 \times 10^{-6} m^3 g^{-1}$. This discrepancy is mostly due to the uncertainty in the refractive index of soot. For instance in the experimental study by Dobbins et al. (1994), at $\lambda = 630nm$ σ_s is reported as 7.8m^{2}g^{-1}. They could get the same

value from their theoretical computation by setting the refractive index $m = 1.55 + 0.780i$. Using $m = 1.55 + 0.780i$ in (14), we get $\sigma_s = 7.4m^2 g^{-1}$. This small difference is possibly due to the simplified expression used by Dobbins et al. (1994) to compute the total scattering cross section. However in this work the extinction is not significant and the slight error in its computation can be disregarded. Our choice of the refractive index ($m = 1.54 + 0.48i$) probably leads to some error in the computation of the angular scattering as well. Due to uncertainty in the value for the refractive index for smoke, this error is not easy to quantify.

Since the scattered intensity is not exactly computed but is obtained from a quadrature approximation, it is necessary to test its accuracy. As mentioned earlier, due to negligible effects of agglomeration, the distribution does not change (i.e. remains lognormal) and therefore higher moments can be calculated from any three moments. Results shown in Fig. 9 for the angular variation of scattered power show that there is a trivially small difference between two-point and higher point approximations. This is remarkable considering that the intensity has an M_6 dependence which is very accurately approximated using moments up to M_4 as in the 2-point scheme. In more realistic simulations of smoke detectors, there may be more complex flow and diffusion effects and arbitrary size distribution of smoke. The accuracy of low order moment approximations would greatly simplify the simulations.

3.4 Detector response study

The objective of any analysis on smoke detectors or other similar geometries is to predict the detector response time. While the analysis presented above enables the computation of the scattered light power falling on the photodiode, a translation of the incident power to a detector signal is required. In a typical operation, the photodiode converts the power into an electric current that upon reaching a certain threshold value, causes the alarm to sound. The relation between the incident power and the output current is usually linear but the threshold current depends on the electronics and varies widely. Consequently, for a theoretical study, an arbitrary choice must be made. In this study we assume that a photodiode is placed at an angle of 20° to the incident beam in the scattering plane (cf. Fig. 3). A fixed value for the incident power per unit power of the source (LED) (hereafter referred to as the critical power, P'_{cr}) is chosen as the threshold criterion. Then the time taken to reach this critical value is assumed to be the detector response time. Another empirically based method has been suggested by Mulholland (1995). It involves use of a detector response function, $R_{det}(d)$, which when integrated over the size distribution gives the detector output voltage. To compare with the calculations based on the light scattering analysis, we use a correlation for $R_{det}(d)$ developed for a particular photoelectric smoke detector in Mulholland and Liu (1980). We evaluate the output voltage, p, by integrating over the smoke size distribution in the same scattering volume (i.e. along the LED beam).

$$p = \frac{1}{2R} \int_{s'=0}^{2R} \int_{\overline{d}=0}^{\infty} R_{det}(\overline{d}) n(\overline{d})(s') d\overline{d} ds' \tag{19}$$

$$R_{det}(\overline{d}) = 1312 \overline{d}^{5.7} \tag{20}$$

The integral for p in equation (19) is computed by a quadrature sum using the known quadrature points and weights. For this particular model, detector sounds when $p \geq 2$ volts (Mulholland and Liu (1980)).

Fig. 10 is the log-log plot showing the variation of the activation time with the velocity. Due to the arbitrary choice of the threshold signal only the comparison of the trends are meaningful. Calculations for t_{act} using the scattering computations closely match the calculations using the detector response function for $P'_{cr} \approx 10^{-6}$. As P'_{cr} increases to around 10^{-6}, there is a slight deviation from the power law behavior at around $U_e \sim 0.1 \mathrm{m/s}$. For lower values of P'_{cr}, the light scattering calculations reveal a power law variation of the activation time, t_{act}, with velocity, U_e, given by $t_{act} \sim CU_e^{-1.12}$. The data for the entire range of velocities for different threshold criteria can be fit reasonably well with a power law given by $t_{act} \sim CU_e^{-m}, m \approx 1$, with a prefactor C that varies according to the threshold intensity criterion. These results indicate that at least for this particular geometry, a simple scaling for the mixing time as $t_{act} = \dfrac{L}{U_e}$ may be adequate.

Fig. 11 shows the comparison of the detector response time with the smoke volume fraction at the inlet. The trends using the two different calculation procedures are again similar for $P'_{cr} \approx 10^{-6}$ for a wide range of inlet volume fractions. The two curves begin to deviate at very low volume fractions ($f_v \sim 10^{-10}$ onwards). At lower P'_{cr}, the light scattering computations show a power law for the activation time in terms of the volume fraction as $t_{act} \sim Cf_v^{-0.09}$. However as P'_{cr} is increased, the power law is only applicable at higher volume fractions. For example Fig. 11 shows that with $P'_{cr} = 10^{-7}$, the power law

scaling begins to break down at $f_v \sim 10^{-9}$ and for $P'_{cr} = 10^{-6}$, it breaks down at $f_v \sim 10^{-8}$. For these cases, the response time increases faster than a power law for decreasing volume fractions. The same trends for the activation time calculated using two different methods is expected provided the threshold power and the threshold voltage are compatible. The criteria for activation computed using (19) depends on the $M_{5.7}$ moment. The moment dependency for the light scattering is not so easy to evaluate. For the Guinier regime (small qR_g), equation (17) gives an $M_6 - \frac{q^2}{3}M_{6+\frac{12}{D_f}}$ dependence for the scattered intensity at a particular angle. For the power law regime (large qR_g) again an M_6 dependence is expected. If the smoke sample contains only small particles or if q is small (i.e. small scattering angles), then the scattered intensity $\propto M_6$. In this case it is reasonable to expect similar trends for the activation time. An interesting observation from Fig. 11 is that for the range of inlet velocity and volume fraction where a power law behavior is applicable, the value of the exponent is almost the same for all the curves.

The CFD analysis and the light scattering computation allow a check for the validity of the assumptions leading to equation (3). Equation (3) is a model for a perfectly stirred mixing process. The volume fraction is proportional to the mass concentration and so (3) can be rearranged to give the following

$$\frac{t - t_e}{\tau_{mix}} = -\ln\left(1 - \frac{f_v(t)}{f_{v\infty}}\right) \tag{21}$$

There are two unknowns t_e and τ_{mix}. The characteristic mixing time τ_{mix} can be determined by computing an average volume fraction $\bar{f}_v$ obtained from CFD calculations

(given by $\bar{f}_v(t) = \dfrac{1}{V_{cav}} \int_{V_{cav}} f_v(\vec{x},t) dV_{cav}$) for the entire cavity and fitting the variation of

$\dfrac{f_{v\infty} - \bar{f}_v(t)}{f_{v\infty}}$ with an exponential curve. The results shown in Fig. 12 show a very good

agreement with the basic model (3) for the entire range of inlet velocities. The data from

Fig. 12 shows that τ_{mix} scales as $\tau_{mix} \sim 20.3 U_e^{-0.97} \approx 20.3 U_e^{-1}$. Comparison with equation

(4) shows that $L_{mix} = 20.3m$ for this particular geometry. For a chosen fixed velocity, the

mixing time τ_{mix} can then be obtained. Supposing there is a single critical volume fraction

for detector activation $f_v(t_{act})$, then t_{act} can be computed as a function of inlet volume

fraction using (21). We fix $f_v(t_{act})$ for each case by assuming this relation holds for

$f_{v0} = 10^{-10}$ and using t_{act} computed from the CFD simulation. The other unknown

parameter, t_e, is obtained by a best fit of the data for t_{act} (obtained from direct

simulations) to equation (21). Fig. 13 shows a plot of activation time with external

volume fraction calculated using (21) for free stream velocity of 0.1 m/s and 1m/s. It is

seen that the detector activation times calculated using (21) are very similar to the

activation times obtained using the full CFD and light scattering model. Further under the

assumption that t_e is specified as in equation (2), values of L_e between 0.3m and 0.35m

give the best fit for a wide range of inlet velocities. These values are of the order of the

maximum size of the computational model (Fig. 2). However the most obvious choice of

$L_e = L/2$ with L being the maximum size of the computational domain shown in Fig. 2

does not give a good fit.

Fig. 6 shows that smoke volume fraction is not uniform inside the cavity, especially at short times when the detector activates. Even though the spatial and temporal distribution of smoke inside the cavity is not homogeneous, for this particular geometry, the two parameter first order model given by (2) and (3) is seen to work very well for the prediction of detector activation time.

The size distribution of the smoke that enters the detector can be quite different from the size distribution of the smoke at the location of the fire due to agglomeration during the transit from the fire to the detector. In Fig. 14, we plot the variation in activation time with volume fraction for different geometric mean radius and geometric standard deviation. For larger volume fractions there is no difference in the activation time while for smaller volume fractions $f_v \sim 10^{-10}$, some differences can be seen. We see that the activation time is almost independent of the geometric mean radius, r_g, as the geometric standard deviation, σ_g, (polydispersity) becomes higher. For the monodisperse case and for lower values of σ_g, it is seen that detector activation time decreases with increasing r_g. The activation time decreases with increasing polydispersity due to the increased scattering from the larger sized particles. However, the differences are not substantial since the results are plotted on a linear scale. It is important to note that these results apply only for fractal aggregates and differences in aerosol morphology could affect the response time. Computations also showed that detector activation time does not vary significantly with primary particle size.

4. Conclusions

A coupled CFD and aerosol dynamics simulation of smoke entry and accumulation processes in a cylindrical cavity geometry is carried out. The geometry and the flow represent an idealized smoke detector. It is seen that for this configuration, flow processes determine the distribution of smoke inside the cavity. Flow enters the cavity by entrainment, it is pushed up at one side setting up a recirculating flow inside the cavity. The same type of flow is seen for a wide range of inlet velocities. Light scattering calculations are carried out using the RDGPFA model for fractal agglomerates. Attenuation is weak for inlet volume fractions around 10^{-9} and hence the light scattered is also weak. We found that for higher inlet volume fractions (around 10^{-6}), there is pronounced attenuation but the detector responds long before the attenuation effects become significant. Therefore a simple model for the attenuation and scattering that ignores multiple scattering is applicable.

A detailed CFD study has been used to test the validity of the simple mixing model (equation (3)) that is widely used in the empirical characterization of smoke detectors. Our calculations indicate that this model is accurate to predict the average mass concentration or volume fraction inside the cavity as well as the detector response time for mass fractal aggregates. This is especially as the detector response time appears to depend very weakly on the size distribution parameters. Even though the spatial distribution of smoke inside the cavity is not homogeneous, it may still be possible to define a single average volume fraction or smoke concentration as a threshold. However the parameters τ and t_e appearing in the simple model do not seem to be directly related to any geometric length scale of the problem. The manner of entry of the smoke and its spatial variation within the sensing chamber may have to be considered only for the

purposes of designing smoke detectors with faster response times. The results we have obtained are only for a very simple idealized model of a smoke detector. It is necessary to extend the type of analysis presented in this paper to more realistic smoke detector geometries and for different types of smoke to get a clearer understanding of how smoke entry and accumulation affects detector response time. The coupling of a general moment method like QMOM to a computational fluid dynamics package will allow more detailed evaluation of aerosol detector physics. Considering the importance of accurate prediction of smoke detector activation time, it is also desirable to check whether the simple model that is widely used in experimental characterization of smoke detectors is always applicable.

Acknowledgements

References

Benjamin, I., Heskestad G., Bright R., & Hayes T. (1979). *An analysis of environments of fire detectors*. Fire Detection Institute, USA, (pp.37).

Bukowski, R.W., & Averill, J.D. (1998). *Methods for predicting smoke detector activation. Fire Suppression and Detection Research Application Symposium. Research and Practice: Bridging the Gap.* Proceedings. National Fire Protection Research

Foundation. Orlando, FL, (pp.64-72), (available on the World Wide Web at URL: http://fire.nist.gov/bfrlpubs/fire98/art185.html).

Bjorkman, J., Baroudi, D., Latva, R., Tuomisaari, M., & Kokkala, M. (2002). Determination of dynamic model parameters of smoke detectors. *Fire Safety Journal, 37*, 395-407.

Cleary, T., Chernovsky, A., Grosshandler, W., & Anderson, M. (1999). *Particulate entry lag in spot-type smoke detectors.* Fire Safety Science. Proceedings. Sixth International Symposium. International Association for Fire Safety Science (IAFSS). July 5-9,1999, Poitiers, France, International Association for Fire Safety Science, Boston, MA, Curtat, M., Editor, (pp.779-790), (available on the World Wide Web at URL: http://fire.nist.gov/bfrlpubs/fire00/art075.html).

Dobbins, R.A., & Megaridis, C.M. (1991). Absorption and scattering of light by polydisperse aggregates. *Applied Optics, 30(33),* 4747-4754.

Dobbins, R.A., & Mulholland, G.W., Bryner, N.P. (1994). Comparison of a fractal smoke optics model with light extinction measurements. *Atmospheric Environment, 28(5),* 889-897.

Farias, T.L., Koylu, U.O., Carvalho, M.G. (1996). Range of validity of the Rayleigh-Debye-Gans theory for optics of fractal aggregates. *Applied Optics, 35,* 6560-6567.

Fox, R.O. (2003). *Computational models for turbulent reacting flows* (pp. 372-386). Cambridge: Cambridge University Press.

Heskestad, G. (1975). *Generalized characterization of smoke entry and response for products of combustion detectors*, International Conference on Automatic Fire Detection, 7th. Probleme der Automatischen Brandentdeckung. March 5-6, 1975, (pp. 267-310).

Heskestad, G., & Delichatsios, M.A. (1997). *Environments of fire detectors – Phase I: Effect of Fire Size, Ceiling Height and Material, Volume 1 – Measurements.* Factory Manual Research Corporation Technical Report 22427, Norwood, MA..

Heskestad, G., & Delichatsios, M.A. (1977). *Environments of fire detectors – Phase I: Effect of Fire Size, Ceiling Height, and Material, Volume 2 – Analysis.* NBSGCR-77-95.

Ierardi, J.A., & Barnett J.R. (2003). *CFD modelling of aerosol entry in simplified smoke detector geometries.* Fire Safety Science. Proceedings. Seventh (7th) International Symposium. International Association for Fire Safety Science (IAFSS), (pp.1170-1170), (available on the World Wide Web at URL: http://fire.nist.gov/bfrlpubs/fire03/art043.html).

Koylu, U.O., & Faeth, G.M. (1994). Optical properties of overfire soot in buoyant turbulent diffusion flames at long residence times. *Journal of Heat Transfer, 116,* 152-159.

Koylu, U.O., & Faeth, G.M. (1996). Spectral extinction coefficients of soot aggregates from turbulent diffusion flames. *Journal of Heat Transfer, 118,* 415-421.

Loepfe, M., Ryser, P., Tompkin, C., & Wieser, D. (1997). Optical properties of fire and non-fire aerosols. *Fire Safety Journal, 29,* 185-194.

Newman, J.S. (1997). Prediction of fire detector response. *Fire Safety Journal, 29,* 99-112.

McGraw, R. (1997). Description of aerosol dynamics by quadrature method of moments. *Aerosol Science and Technology, 27,* 255-265.

McGraw, R., & Wright, D.L. (2003) Chemically resolved aerosol dynamics for internal mixtures by the quadrature method of moments. *Journal of Aerosol Science, 34,* 189-209.

Mulholland, G.W. (1995) Smoke production and properties. In *SFPE handbook of fire protection engineering, 2nd ed.* (pp. 2-217-27), Quincy, MA: NFPA.

Mulholland, G.W., Liu, B.Y.H. (1980). Response of smoke detectors to monodisperse aerosols. *Journal of Research of the National Bureau of Standards, 85(3),* 223-238.

Nelson, J. (1989). Test of a mean field theory for the optics of fractal clusters. *Journal of Modern Optics, 36,* 1031-1057.

Snegirev, A.Yu., Makhviladze, G.M., & Roberts, J.P. (2001). The effect of particle coagulation and fractal structure on the optical properties and detection of smoke. *Fire Safety Journal, 36,* 73-95.

Sorensen, C.M. (1997). Scattering and absorption of light by particles and aggregates. In Birdi, K.S. (Editor), *Handbook of Surface and Colloid Chemistry* (pp.533-558), CRC Press.

Sorensen, C.M. (2001). Light scattering by fractal aggregates: a review. *Aerosol Science and Technology, 35,* 648-687.

Sorensen, C.M., Cai, J., & Lu, N. (1992). Light-scattering measurements of monomer size, monomers per aggregate and fractal dimension for soot aggregates in flames. *Applied Optics, 31,* 6547-6557.

Sorensen, C.M., & Fischbach, D.J. (2000). Patterns in Mie scattering. *Optics Communications, 173,* 145-153.

Upadhyay, R.R., & Ezekoye, O.A. (2003). Evaluation of the 1-point quadrature approximation in QMOM for combined aerosol growth laws. *Journal of Aerosol Science, 34,* 1665-1683.

Weinert, D.W., Cleary, T.G., Mulholland, G.W., & Beever, P.F. (2003). *Light scattering characteristics and size distribution of smoke and nuisance aerosols.* Fire Safety Science. Proceedings. Seventh (7th) International Symposium. International Association for Fire Safety Science (IAFSS). June 16-21, 2003, Worcester, MA, International Association for Fire Safety Science, Boston, MA, Evans, D. D., Editor(s), (pp. 209-220), (available on the World Wide Web at URL: http://fire.nist.gov/bfrlpubs/fire03/art058.html).

Widmann, J.F. (2003). Evaluation of the Planck mean absorption coefficients for radiation transport through smoke. *Combustion science and Technology, 175*, 2299-2308.

Wright, D.L., McGraw R, & Rosner, D.E. (2001). Bivariate extension of the quadrature method of moments for modeling simultaneous coagulation and sintering of particle populations. *Journal of Colloid and Interface Science, 236,* 242-251.

Wright, D.L. (2000). Retrieval of optical properties of atmospheric aerosols form moments of the particle size distribution. *Journal of Aerosol Science, 31,* 1-18.

Table 1

Summary of the boundary conditions used in the flow and aerosol dynamics simulation.

(Boundaries are labeled in Figure 2.)

Boundary	Flow Boundary Condition	Aerosol Boundary Condition
I	Fixed Inlet Velocity	Fixed inlet moments (lognormal distribution).
II	Symmetry	Symmetry
III	Constant pressure (Atmospheric pressure)	Zero gradients for the moments in flow direction $\vec{V} \cdot \nabla M_m = 0, m = 0,1,2,3;$
IV	Wall (no slip)	Perfectly absorbing wall $M_m = 0, m = 0,1,2,3$
V	Symmetry	Symmetry
VI	Wall (no slip)	Perfectly absorbing wall $M_m = 0, m = 0,1,2,3$
VII	Wall (no slip)	Perfectly absorbing wall $M_m = 0, m = 0,1,2,3$

List of figures

Fig. 1. Schematic illustrating the first order, two parameter smoke detector model.

Fig. 2. Geometry and computational grid. Flow direction is shown and the boundaries are labeled and referred to in Table 1.

Fig. 3. Schematic of the light scattering arrangement.

Fig. 4. (a) X- and Z- velocity vector components at the plane of symmetry at Y=0.0, (vector lengths are equal and do not show the magnitude). (b) Z- velocity component at the plane of symmetry at Y=0.0.

Fig. 5. Plots of X-Y velocity vectors at the four different horizontal planes at Z=0.0m, Z=0.025m, Z=0.05m and Z=0.075m. Z-velocity contours are also shown.

Fig. 6. Variation of volume fraction with distance at the mid height of the cavity for various times. Volume fraction of the free stream is 10^{-9}.

Fig. 7. Variation of normalized intensity with distance at the mid height of the cavity for various times. Volume fraction of the free stream is 10^{-9}.

Fig. 8. Variation of scattered power at the circumference of the cavity with angle at mid-height for different times. Volume fraction of the free stream is 10^{-9}.

Fig. 9. Comparison of the angular scattering computed using 2-point, 3-point and 4-point quadrature approximations. Differences are too small for the three profiles to be distinguishable.

Fig. 10. Log-log plot showing the variation of the detector activation time with velocity at the inlet. Comparison of the results obtained using the light scattering calculation (equation 18) and the detector response function (equation 19) for different choices of the threshold power.

Fig. 11. Log-log plot showing the variation of the detector activation time with smoke volume fraction at the inlet. Comparison of the results obtained using the light scattering calculation (equation 18) and the detector response function (equation 19) for different choices of the threshold power.

Fig. 12. Plot of the averaged and normalized volume fraction with time for different velocities to evaluate the mixing time scale parameter τ.

Fig. 13. Log-log plot showing the variation of the detector activation time (calculated using equation 18) with smoke volume fraction at the inlet, free stream velocity is 0.1m/s

and 1m/s. Also shown are the best fits of the data to equation 21 obtained from the simple model (equation (3)).

Fig. 14. Plot of the activation time with logarithm of the volume fraction for different values of the geometric mean radius and the geometric standard deviation. The free stream velocity is 0.1 m/s.

.

Smoke Detector Housing

C_{so}, U_e, t_e

L_e

Mixing time
τ

$C_s(t)$

Sensing chamber

Plug flow model

Mixing model

Fig. 1.

.

Fig. 2

Fig. 3.

X-Z plane at y=0m.

X-Z plane at y = 0 m. (z-velocity only)

Fig. 4 (a), (b).

Z= 0.0 m

Z = 0.025 m

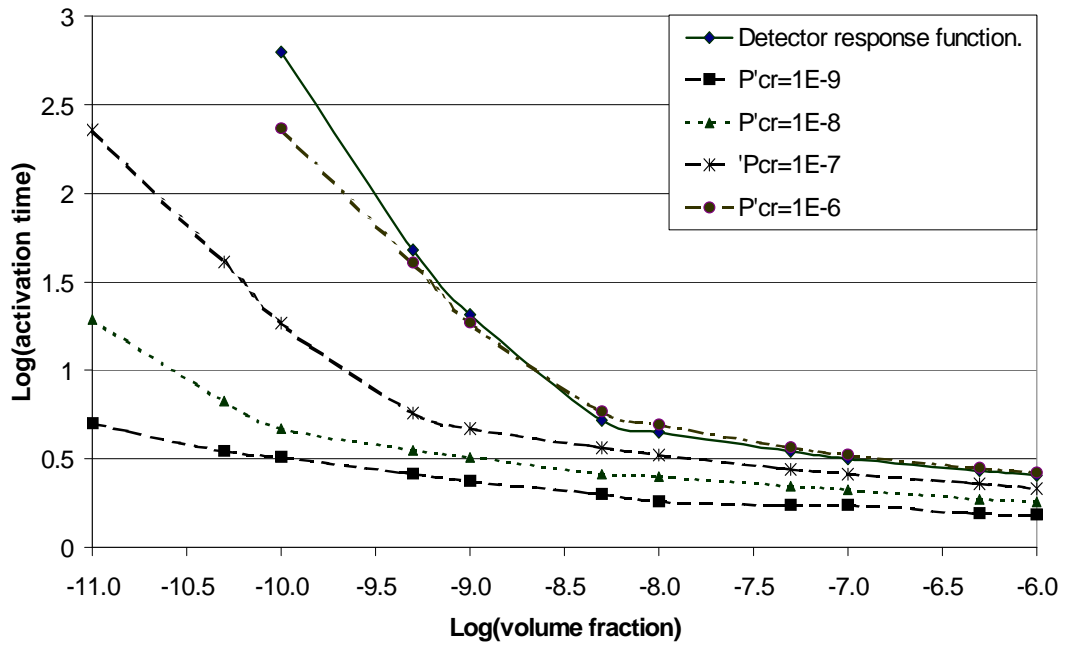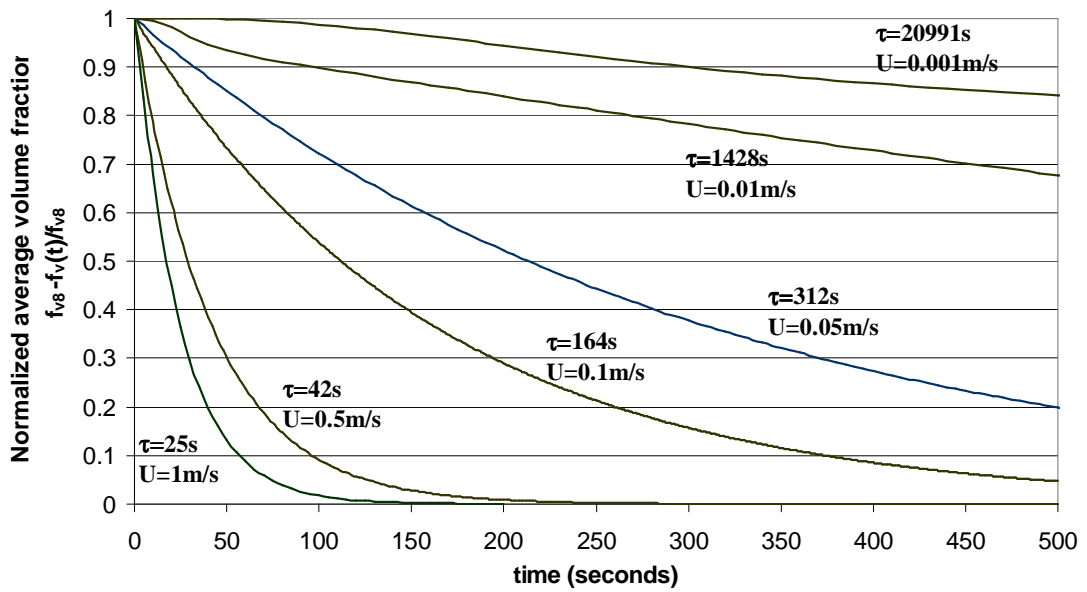**Z = 0.05 m**

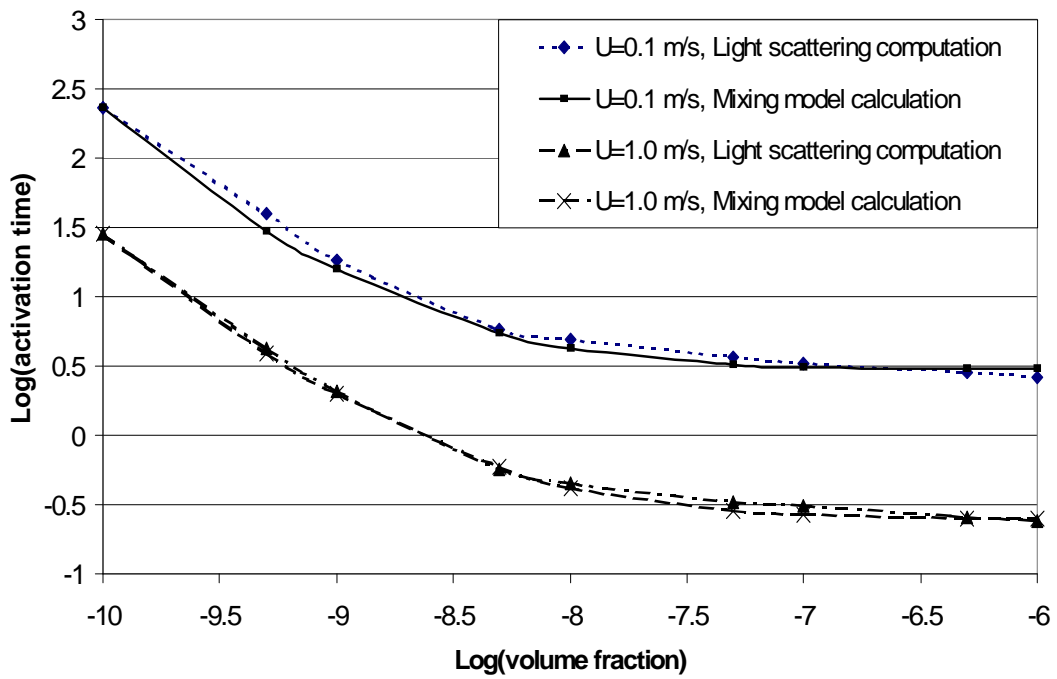**Z = 0.075 m**
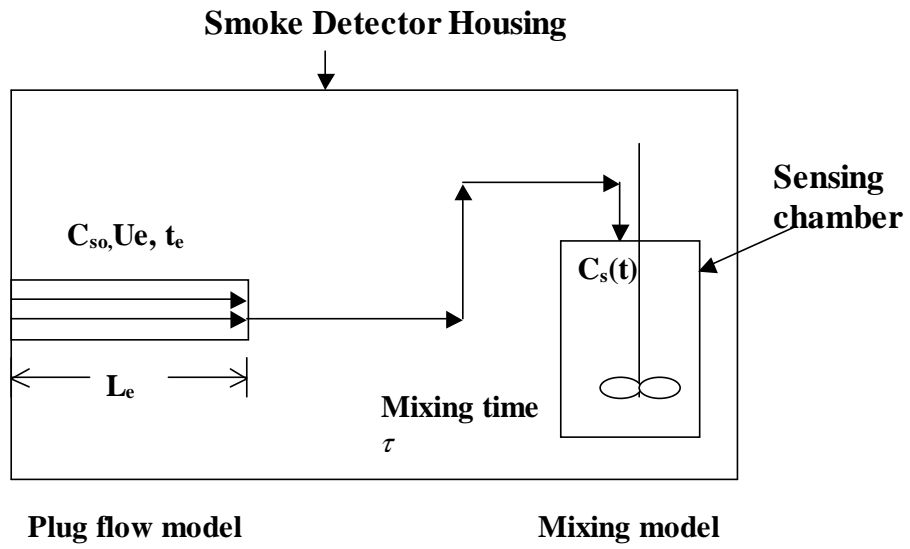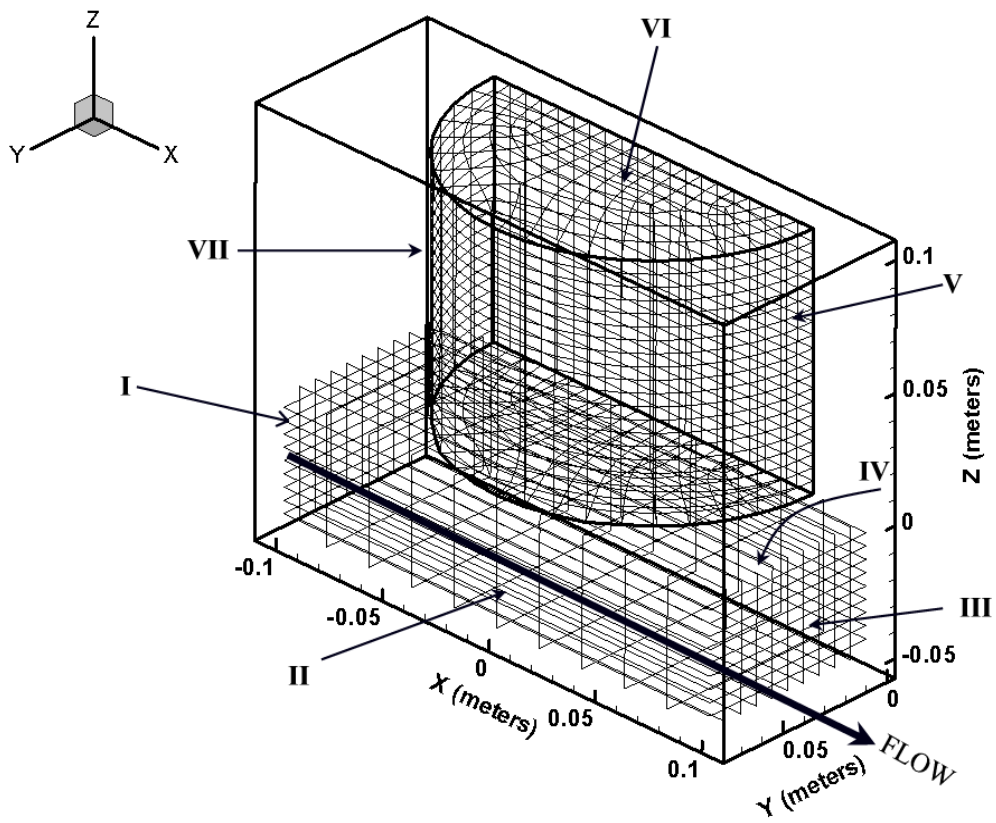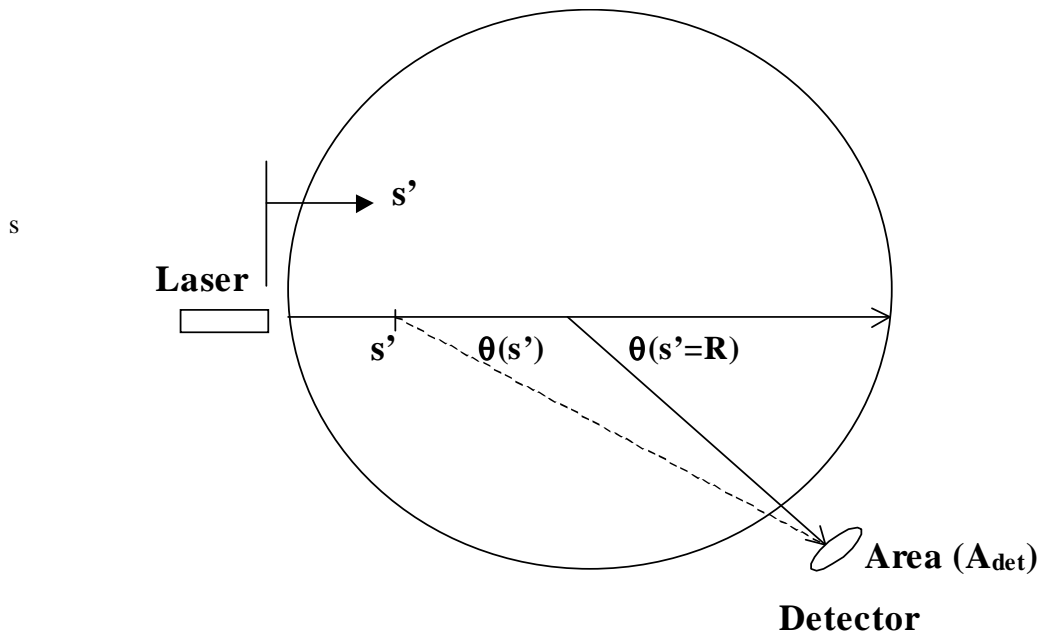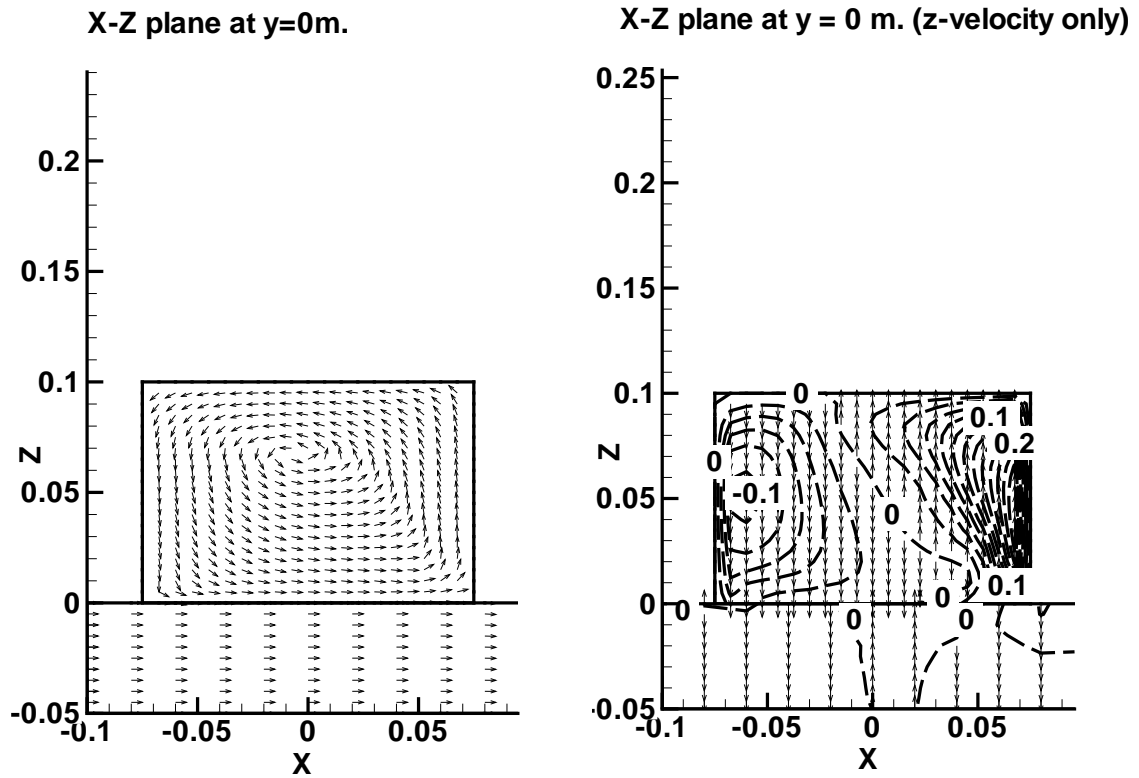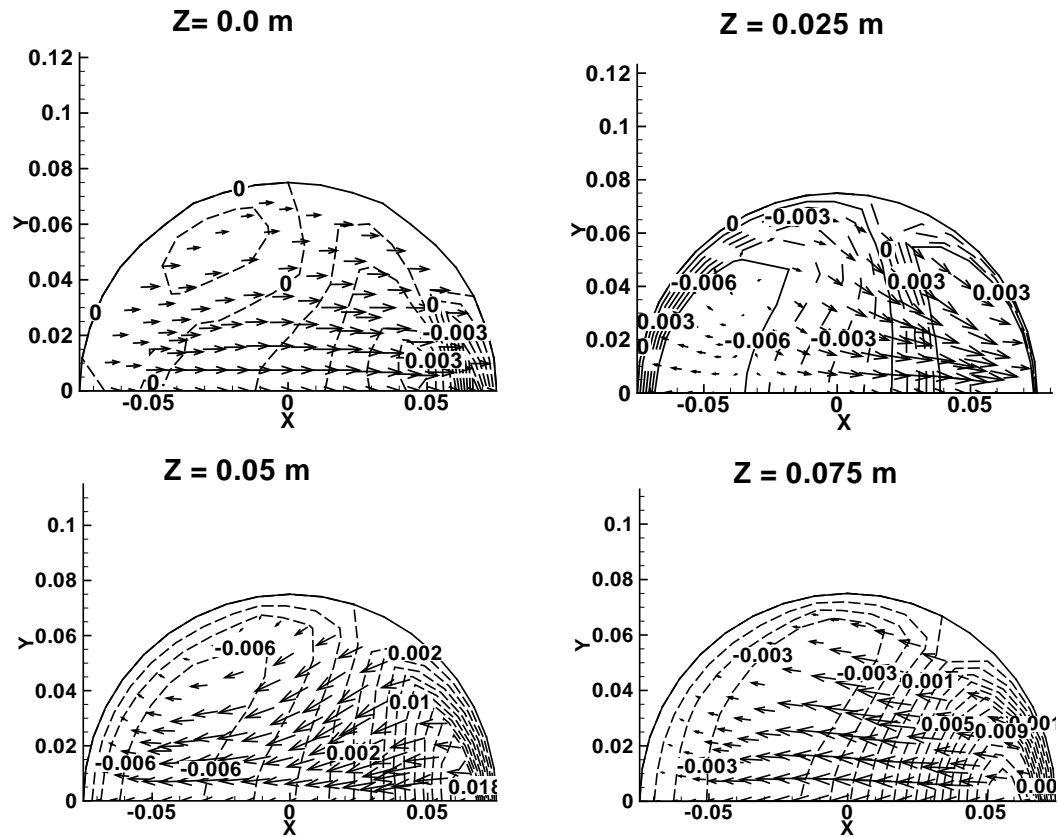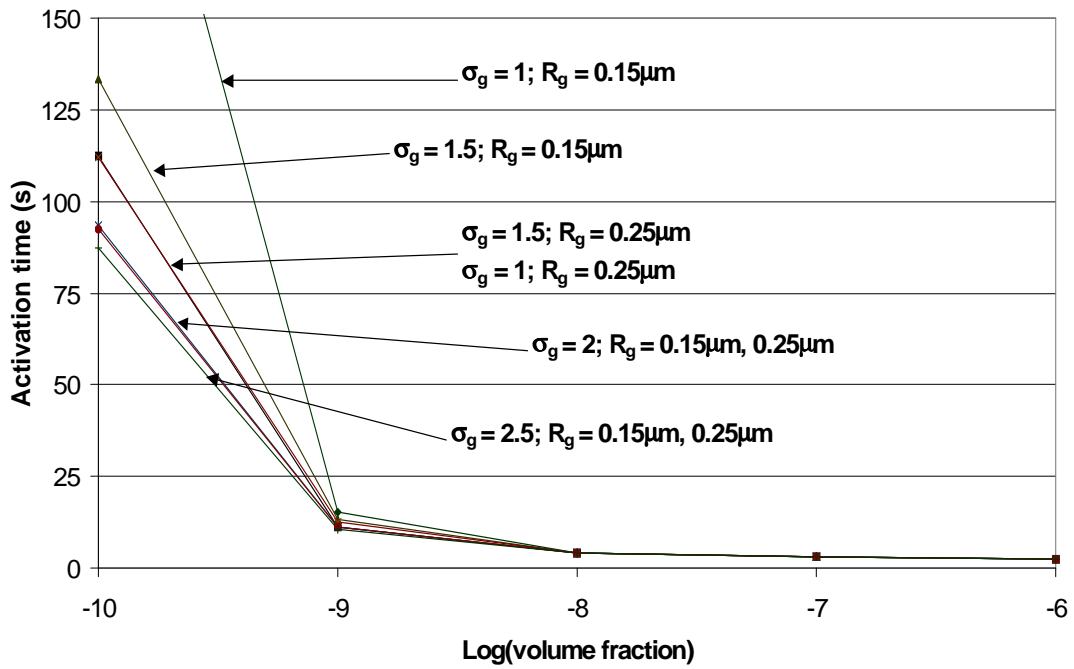
Fig. 5.
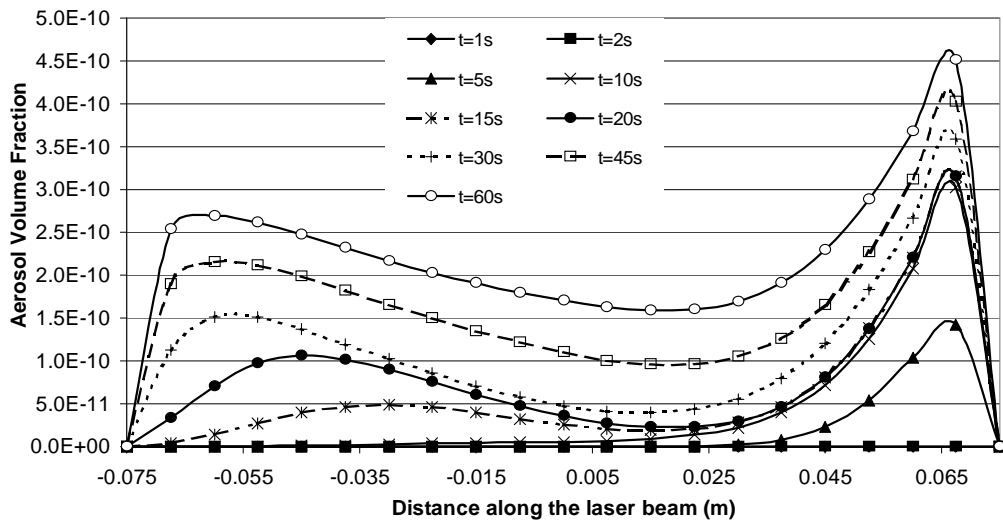
Fig. 6.
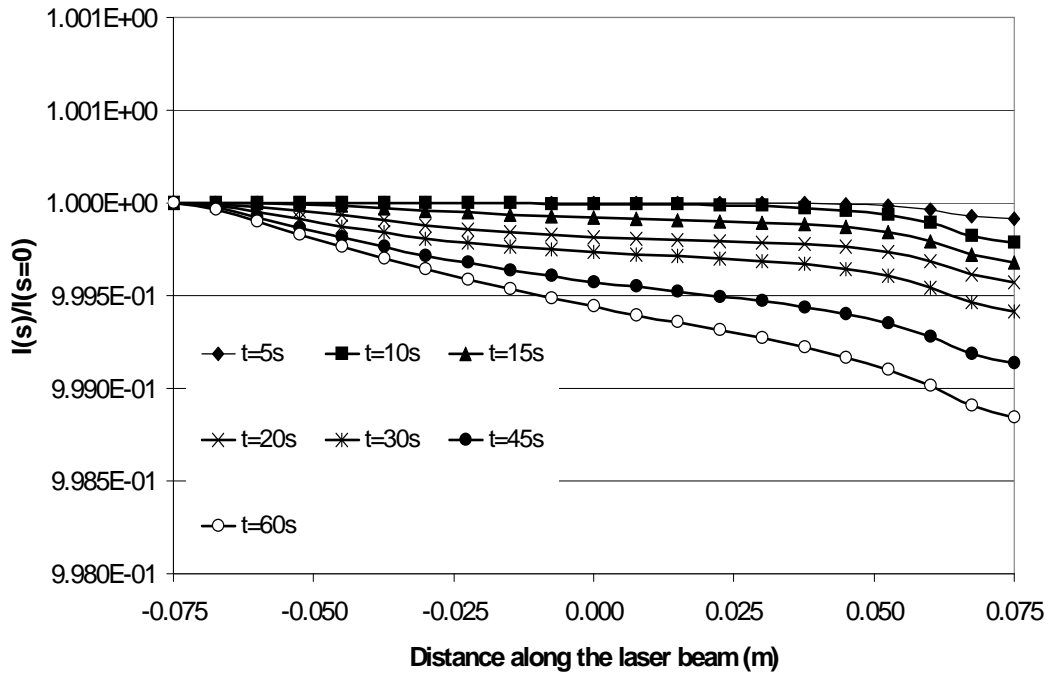
Fig. 7.
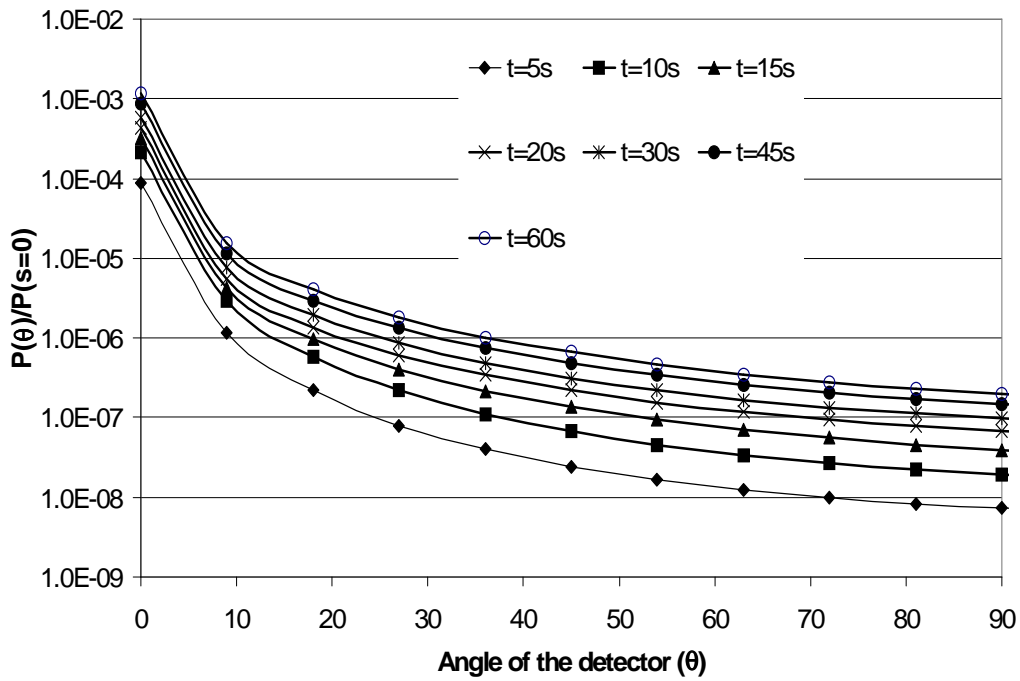
Fig. 8.
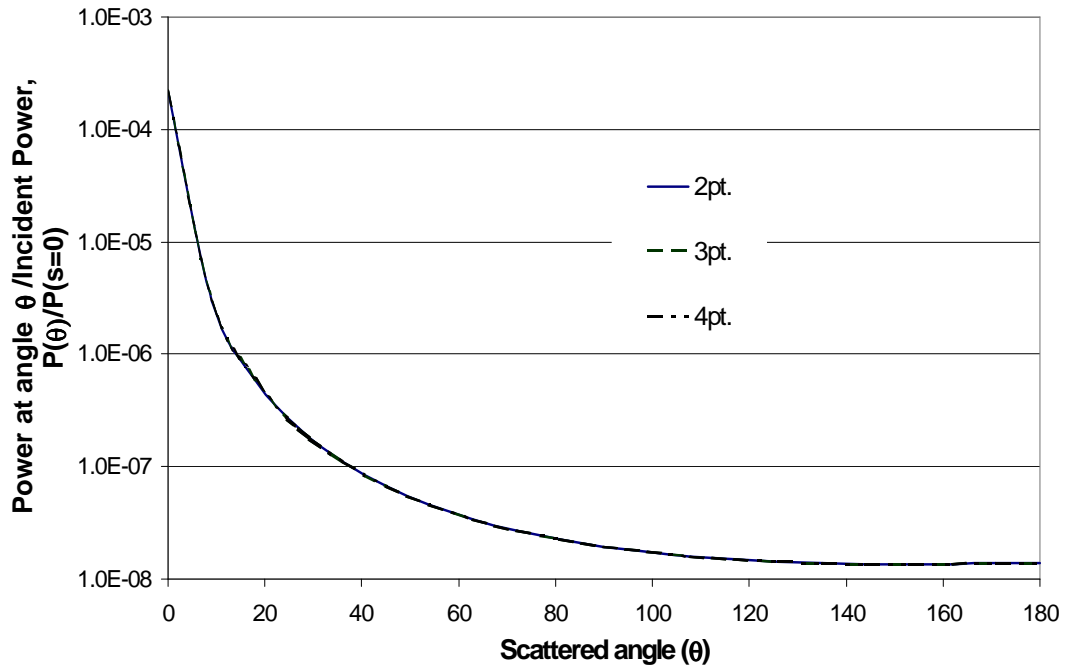
Fig. 9.
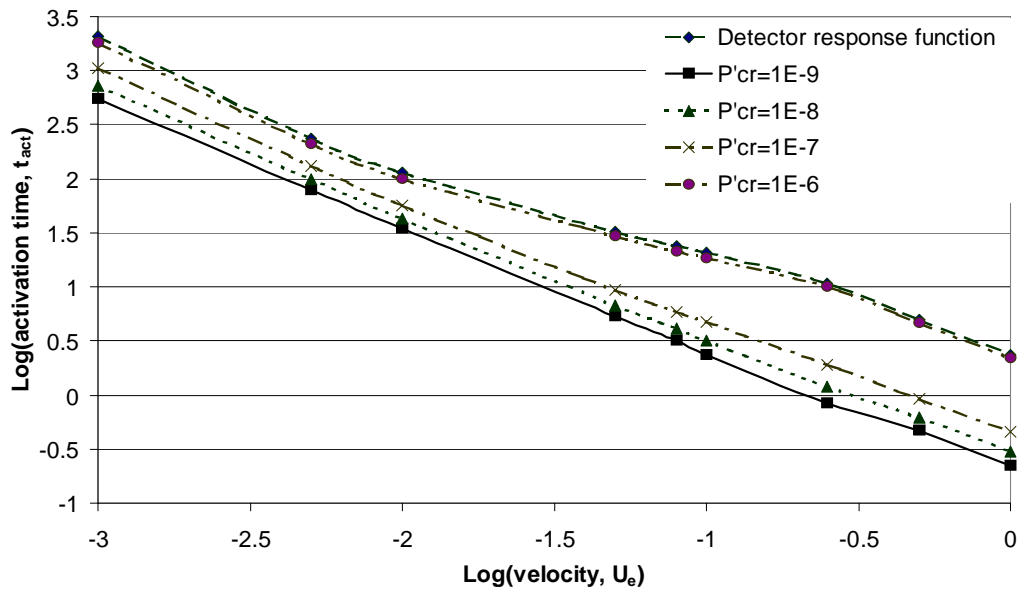
Fig. 10.

Fig. 11.

Fig. 12.

Fig. 13.

Fig. 14.